LUND UNIVERSITY

Influence of cell shape and aggregate formation on the optical properties of flowing whole blood

Enejder, AMK; Swartling, Johannes; Aruna, P; Andersson-Engels, Stefan

[Link to publication](#)

Influence of cell shape and aggregate formation on the optical properties of flowing whole blood

Annika M. K. Enejder, Johannes Swartling, Prakasa Aruna, and Stefan Andersson-Engels

We studied the influence of shape and secondary, or intercellular, organization on the absorption and scattering properties of red blood cells to determine whether these properties are of any practical significance for optical evaluation of whole blood and its constituents. A series of measurements of transmittance and reflectance of light from bovine blood in a flow cuvette was conducted with a 650–900-nm integrating sphere at shear rates of 0–1600 s^{-1}, from which the influence of cell orientation, elongation, and aggregate formation on the absorption (μ_a) and the reduced scattering (μ_s') coefficients could be quantified. Aggregation was accompanied by a decrease of 4% in μ_s' compared with the value in randomly oriented single cells. Increasing the degree of cell alignment and elongation as a result of increasing shear rate reduced μ_s' by 6% and μ_a by 3%, evaluated at a shear rate of 1600 s^{-1}. Comparison with T-matrix computations for oblate- and prolate-shaped cells with corresponding elongation and orientation indicates that the optical properties of whole blood are determined by those of its individual cells, though influenced by a collective scattering factor that depends on the cell-to-cell organization. We demonstrate that cell morphological changes must be taken into consideration when one is conducting whole blood spectroscopy. © 2003 Optical Society of America

OCIS codes: 170.1470, 170.1530, 170.6510, 290.0290.

1. Introduction

A fundamental understanding of the light-scattering and -absorption properties of tissue can be gained by relating optical signals collected from the biological medium to the tissue's chemical and morphological properties on a microscopic level. Here we investigate the influence of cell shape, orientation, distribution, and aggregate formation on the optical properties of blood. Most tissues consist of disparately oriented cells of various sizes and shapes, yielding isotropic scattering properties of bulk tissue. Blood, with its many elastic and uniformly shaped red blood cells (RBCs) without intracellular scattering structures, is in this respect an exception. Cell morphological changes occur collectively and can be induced in a relatively well-controlled and consistent manner. Thus, blood provides a suitable and important medium with which to study the influence of cell morphology on optical properties. A better understanding of these phenomena is highly desirable for the large community of scientists who are developing spectroscopic methods for blood analysis *in vitro* as well as *in vivo* (e.g., to measure oxygen saturation and hemoglobin content and derive quantitative information on various blood analytes such as glucose) as diagnostic tools with a wide range of clinical applications.

Because of the viscoelastic properties of blood, one can readily induce variations in cell shape, size, orientation, aggregate formation, and distribution by changing the shear rate to which cells in motion are exposed. The shear rate is formally a measure of the deformation rate of a fluid element in a viscous fluid and is defined as the velocity gradient in the direction normal to the blood flow. The RBC morphology associated with the applied shear rate, G, has been well documented by means of flash photomicrographs taken in a rheoscope chamber[1,2] and by following the motion of individual RBCs in transparent suspensions of blood cell ghosts.[3] At concentrations that correspond to those of whole blood, the RBCs are arranged in three-dimensional cross-linked networks

A. M. K. Enejder is with the G. R. Harrison Spectroscopy Laboratory, Massachusetts Institute of Technology, 77 Massachusetts Avenue, Cambridge, Massachusetts 02139. J. Swartling (johannes.swartling@fysik.lth.se) and S. Andersson-Engels are with the Department of Physics, Lund Institute of Technology, P.O. Box 118, SE-221 00 Lund, Sweden. P. Aruna is with Anna University, 600 025 Madras, India.

of rouleau strings–spheroids when the fluid is still or is subjected to low shear rates.[4] This network is gradually decomposed into single rouleau formations at low shear rates and eventually into single, randomly oriented, biconcave-shaped cells with increasing shear rate. Schmid-Schönbein *et al.* have shown that the disaggregation of the RBCs is essentially complete for shear rates larger than 100 s^{-1}.[5] This condition is followed by an increasing degree of alignment with the symmetry axis of the disk-shaped cells oriented along the shear direction, i.e., perpendicular to the flow direction and here along the direction of the probe beam.[6] Schmid-Schönbein *et al.* used a shear rate value of 460 s^{-1} to represent a condition of aligned cells.[5] With increasing shear rate the RBCs are elongated to flat prolate-shaped ellipsoids oriented with their symmetry axes along the flow direction.

Changes in cell shape, orientation, degree of alignment, and secondary structure all influence the absorption and scattering properties of blood. These properties are quantified by the absorption and scattering coefficients (μ_a and μ_s, respectively), defined as the probability of absorption or scattering per unit path length of the propagating light. In addition, the angular distribution of the scattered light (described by a phase function or an angular scattering probability function) is determined by anisotropy factor g, defined as the average cosine of the scattering angles. Several phase functions have been suggested for blood, many of which are based on measurements at unphysiologically low concentrations of RBCs.[7,8] However, the Henyey–Greenstein phase function has been shown to match well the angular distribution of the light scattered from whole blood.[9,10] The strength of the optical coefficients mentioned above is that they can easily be translated into measured quantities such as light transmittance and reflectance by means of simple light-propagation models such as a Monte Carlo model.[11] Their relationship to cellular properties cannot so easily be derived but must be determined experimentally. In this study we conducted experiments with flowing blood, using an integrating sphere to determine absorption coefficient μ_a and the reduced scattering coefficient, defined as $\mu_s' = \mu_s(1 - g)$, for various RBC morphologies and employing an inverse Monte Carlo model. When one is evaluating μ_s', in contrast to measuring μ_s, the choice of phase function has been shown to have only minor importance.[12]

In a first approximation, the scattering and absorption coefficients can be regarded as volume densities of the scattering and absorption cross sections (σ_s and σ_a) of the RBC, which are directly influenced by the cell size, shape, and orientation relative to the incident wave. Thus a quantitative comparison between the experimentally obtained optical coefficients and the theoretically derived optical cross sections is interesting. The latter can be determined by light-scattering computations of the RBC as a single-scattering particle with appropriate size and shape. Here, T-matrix theory[13] was used to gener-
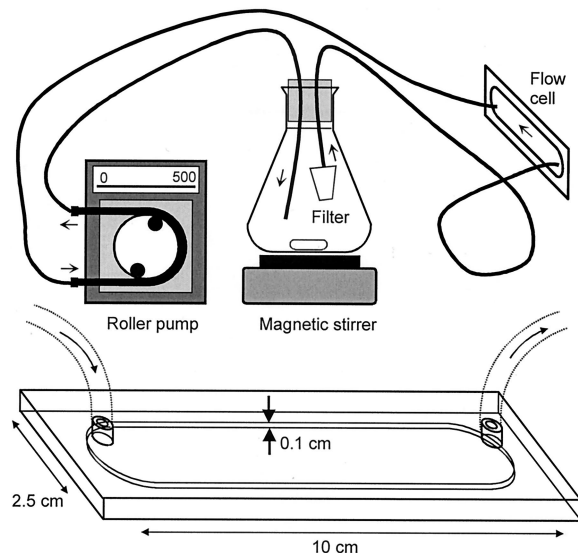

Fig. 1. Schematic of the flow setup in which the blood was circulating: a flask and a cuvette, connected by PVC tubing. A detailed drawing of the cuvette is also shown.

ate scattering and absorption cross sections of individual bovine RBCs. However, in whole blood, which has a volume fraction [hematocrit (Hct)] of RBCs of 0.4–0.45, collective scattering effects become increasingly important. The result is a reduction of the scattering and the absorption power at an intercellular spacing of less than approximately three radial distances.[14] Thus a comparison of the single-scattering cross sections with experimentally obtained scattering and absorption coefficients gives a first rough estimate of the importance of collective scattering effects in whole blood that previously was shown theoretically.[14]

The experimental equipment used to measure the optical properties of flowing blood is described in Section 2. In Section 3 the inverse model that we used to determine μ_a and μ_s' based on Monte Carlo simulations of whole blood as a multiple scattering medium is described, as well as the T-matrix method for generating the absorption and scattering cross sections of single RBCs. In Section 4 an overview of, and a motivation for, the experiments is provided. Results are shown in Section 5. These results are discussed in Section 6, and conclusions are given in Section 7.

2. Equipment

A. Blood Circulation

Bovine blood was circulated at ambient temperature (~ 22 °C) through an optical cuvette, as illustrated in Fig. 1. The circulation system consisted of an airtight 300-ml E flask, with a magnetic stirrer spun at slow speed to prevent sedimentation. The blood was pumped by a peristaltic roller pump (BP101A, Gambro Lundia AB, Sweden) from the blood reservoir to the optical flow cuvette via disposable PVC tubing (4-mm inner diameter; Gambro Lundia AB, Sweden),
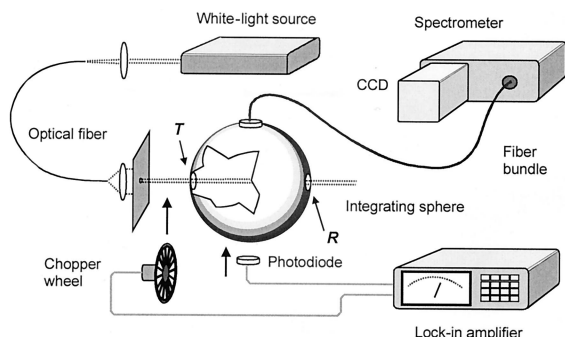
Fig. 2. Optical setup with the integrating sphere and the two detection systems: the spectrometer–CCD camera for spectral measurements and the photodiode–lock-in amplifier for faster data sampling. The transmitted and reflected light was measured with the cuvette placed in position T and R, respectively.

designed for hemodialysis use. A filter was mounted in the flow path to collect any blood clots. The flat rectangular flow cuvette had a size of 10 cm (length) × 2.5 cm (height) × 1.0 mm (thickness). It was made from transparent PVC with a single wall thickness of 3 mm, rigid enough to ensure a constant optical path length. The range of flow rates that could be delivered by the pump was 50–500 ml/min, corresponding to shear rates of 200–2000 s^{-1} at the wall of the cuvette. The shear rate at position $y(-t/2 < y < t/2)$ from the center in a duct of rectangular cross section is given by

$$G_{\text{rect}}(y) = \frac{\mathrm{d}U(y)}{\mathrm{d}y} = \frac{12Qy}{ht^3} \qquad (h \gg t) \qquad (1)$$

for a parabolic velocity profile (Poiseuille flow)[15] with thickness t, height h, and volumetric flow Q.

B. Imaging of Transmitted Light

Images of the light transmitted through the cuvette were collected with a cooled 330 × 1100 pixel CCD camera (TEA/CCD-1100-PB, Princeton Instruments, Trenton, N.J.). A He–Ne laser (15 mW; Coherent, Santa Clara, California) at 633 nm was employed as the light source. Lenses were arranged to produce a laser spot size large enough to cover the entire flow cuvette, and the camera was placed on the opposite side of the cuvette. Screens were carefully mounted around the cuvette to prevent any direct laser light from entering the camera.

C. Integrating Sphere Setup

The transmittance and reflectance spectra were collected by means of an optically integrating sphere (Oriel Corporation, Stratford, Conn.) as described in detail in Ref. 16. Figure 2 illustrates the optical arrangement. A 100-W halogen lamp provided the probe light, which was collimated to a beam diameter of 4 mm at both sample positions (reflectance and transmittance positions) of the integrating sphere. The light collected from the sample was collected by the sphere and further guided by an optical fiber bundle to a spectrometer (270M, SPEX Industries,

Inc., Edison, N.J.). A cryo-cooled CCD camera (OMA-Vision, EG&G PARC, Princeton, N.J.), with 512 × 512 pixels vertically binned, was used for detection. With this arrangement, wavelengths of 650–900 nm could be detected at a spectral resolution of ~4 nm. From the measured values, the transmittance (T) and reflectance (R) were obtained at each wavelength by

$$T = I_T/I_{\text{ref}}, \qquad (2)$$

$$R = R_{\text{BS}}(I_R/I_{\text{ref}}), \qquad (3)$$

forming transmittance and reflectance spectra. The notation I_T is used for the intensity measured with a sample kept at the entrance port of the sphere together with a highly reflecting barium sulfate plug at the exit port. Intensity I_R was measured when the sample was positioned at the exit (reflectance) port with the entrance port open. Reference intensity I_{ref} was measured with the reference plug at the exit port only. The property R_{BS} refers to the tabulated reflectance of the calibrated barium sulfate reference plug. Light losses that are due to the finite size of the integrating sphere ports may be of concern when one is measuring R and T. In this study, however, such losses are negligible because of the strong absorption of light by the samples (whole blood).

Alternatively, a photodiode was mounted at the detection port of the integrating sphere and connected to a lock-in amplifier (SR830, Stanford Research Systems, Sunnyvale, Calif.). This arrangement facilitated faster data sampling, though at the sacrifice of spectral information. The light beam from the halogen lamp was modulated at 1.38 kHz by a mechanical chopper wheel for lock-in detection. This method, also shown in Fig. 2, permitted highly accurate measurements to be made at a time constant of 1 s. An IR filter was used to block out most of the light above 900 nm from the lamp. Thus the spectral range covered by the photodiode corresponds well to that covered in the spectrally resolved measurements.

3. Models

Two types of model for light propagation and scattering were employed in this study. First, we used an inverse model based on Monte Carlo simulations of whole blood as a multiple scattering medium to determine absorption coefficient μ_a and reduced scattering coefficient μ_s' from the integrating sphere measurements.[16] Second, we performed T-matrix computations for single spheroid particles that resembled RBCs of various shapes to yield scattered field distributions as well as the corresponding scattering and absorption cross sections. The T-matrix results were then compared with the experimentally obtained values of μ_a and μ_s' for the various cell morphological conditions.

A. Inverse Monte Carlo Method

The inverse Monte Carlo method of generating μ_a and μ_s' from the measured values T and R [Eqs. (2)

and (3)] was previously.[16] It is based on the Monte Carlo simulation program MCML by Wang *et al*.[11] We traced 2×10^5 photon packages per run with input parameters in the ranges 0.1–2.5 mm^{-1} for the absorption coefficient and 0.5–2.5 mm^{-1} for the reduced scattering coefficient. The scattering anisotropy factor was fixed at $g = 0.99$, and the Henyey–Greenstein phase function was applied for all simulations. A database of the T and R values that we obtained was built and used as a lookup table. The optical properties μ_a and $\mu_s{}'$ were then deduced from the measured quantities T and R by use of a two-dimensional spline interpolation algorithm.

The influence of the PVC walls of the flow cuvette on the light transmittance and reflectance was incorporated in the database simulations. Thus there was no need for additional calibration of the measurements to allow for the influence of the cuvette. The light transmittance through the PVC layer alone was measured to be 90%, and, within a few percent, remained constant over the wavelength range of interest. The refractive index was 1.52, which we determined for red light by measuring the optical path length through a PVC sheet with a microscope.

B. T-Matrix Computations

Computations were made of the light-scattering probability $P(\theta, \phi)$, where θ and ϕ are the zenith and the azimuthal scattering angles, respectively, of a spheroid with a volume equivalent to that of a bovine RBC (40.4 μm^3) at the wavelength 800 nm.[17] The T-matrix code of Barber and Hill,[13] modified for double and extended precision variables,[14] was employed. Based on the average concentration of hemoglobin in the bovine RBCs (370 g/l),[17] the real and imaginary parts of the refractive index were calculated to be 1.412 and 8.221×10^{-5}, respectively, from formulas derived by Tycko *et al*. for the wavelength 842 nm.[18] The difference in wavelength of 42 nm compared to the 800 nm employed here is not expected to influence the refractive index significantly. Based on these input data, the scattering and absorption cross sections (σ_s and σ_a) for individual spheroids were generated by the T-matrix computations. In addition, the g factor was calculated from the angular scattering probability obtained:

$$ g = N \iint P(\theta, \phi)\cos(\theta)\sin(\theta)\mathrm{d}\theta\mathrm{d}\phi, \qquad (4) $$

where N is the normalization constant of $P(\theta, \phi)$. To estimate the effect of cell alignment on the optical properties of a RBC observed with increasing shear rate, we computed σ_s, σ_a, and g for an oblate-shaped spheroid with its symmetry axis oriented at 0, 15, 30, . . . , 90 deg relative to the incident beam, as exemplified in Figs. 3(a) and 3(b). Radius a along the symmetry axis of the spheroid was 1.543 μm, and radius b, which was perpendicular to a, was 2.5 μm, corresponding to a size parameter, $x_{\mathrm{spheroid}} = 2\pi a/\lambda$, of 16.4 and an aspect ratio $\varepsilon = a/b$ of 0.62. The condition of randomly oriented cells (preceding the

cell alignment) was modeled as a power-law size distribution of spheres:

$$ f(x) = \frac{\varepsilon^4 x_{\mathrm{spheroid}}^5}{(\varepsilon^2 - 1)x^5} \left(\frac{\varepsilon^2 - 1}{x_{\mathrm{spheroid}}^2 \varepsilon^2 - x} \right)^{1/2}, \qquad (5) $$

with size parameters ranging from $2\pi a/\lambda$ to $2\pi b/\lambda$. Shepelevich *et al*. have proved that such a distribution of spheres is equivalent to a system of randomly oriented spheroids with the real part of the refractive index close to that of the surrounding medium.[19] This condition is fulfilled for RBCs in plasma. We modeled the formation of randomly oriented rouleau strings in conjunction with the aggregation process as long prolates consisting of 2–15 stacked RBCs, again employing the power-law distribution approach. This modeling method was justified by computations showing negligible influence of the RBC membrane on scattering properties.[20,21] Finally, we modeled the elongation of one of the major radii of the cell by increasing the radius along the symmetry axis of a prolate spheroid, conserving the spheroid volume to that of a bovine RBC [Fig. 3(c)]. Spheroids with radii of 2.5–2.65 μm (0–6%) were investigated. Here, data will be exemplified for a prolate with an increase of 5% of the radius (2.625 μm) along the symmetry axis and related to the properties of a nonelongated prolate (2.5 μm). The size parameters were 27.8 (elongated) and 26.5 (nonelongated), and the corresponding aspect ratios were 1.37 and 1.27.

4. Experiments

Whole bovine blood, circulating through an optical cuvette as illustrated in Fig. 1, was studied in three separate experiments. First, the distribution of RBCs across the cuvette was investigated. The laminar and homogeneous character of the flow had to be ensured for the subsequent experiments. The uniformity of the distribution was not obvious because of the instant change in flow geometry at the inlet and the outlet of the cuvette: from a circular to a thin, rectangular cross section. The homogeneity of the cell distribution was evaluated from spatial variations of the light transmittance through the cuvette, recorded by means of the CCD camera.

In the second experiment, spectral measurements of transmittance T and reflectance R were conducted in the central cuvette region by means of an optically integrating sphere. We studied the influence of RBC orientation and elongation on μ_a and $\mu_s{}'$ by continuously increasing the shear rate. Under the guidance of the observations made by Schmid-Schönbein *et al*.,[5] we used the values obtained at 400 s^{-1} to signify the condition of aligned RBCs. The values obtained at the maximum shear rate that was employed (1600 s^{-1}) were taken to represent the condition of elongated cells. The two optical properties were deduced from the parameters measured by use of the inverse Monte Carlo model.

In the third experiment, T and R were recorded over time by lock-in detection. The objective was to monitor possible changes in optical properties in con-

(a)

(b)

(c)
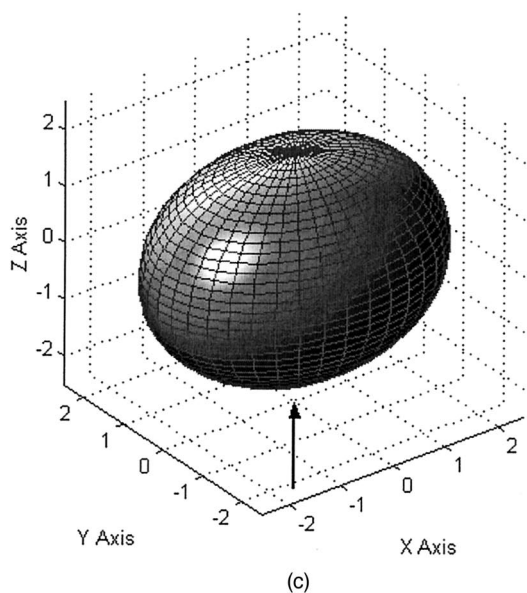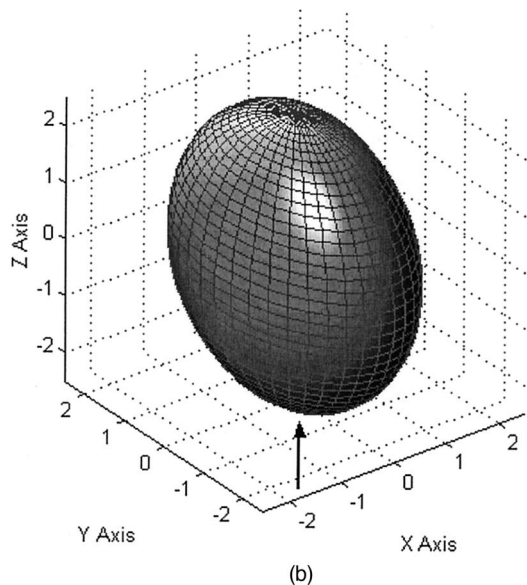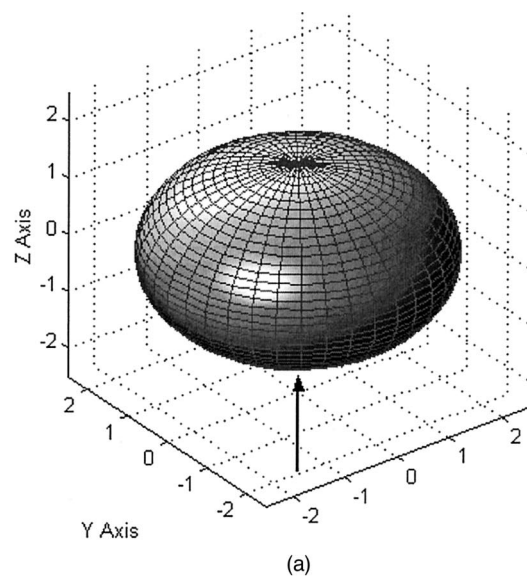
junction with the aggregate formation in the transition from flowing to stationary conditions, at a higher sampling rate than that offered by the spectrometer–CCD camera. This was accomplished at the expense of the spectral resolution. The results of these measurements were also evaluated by use of the inverse Monte Carlo model.

A. Monitoring Blood Parameters

Fresh bovine blood from healthy animals was collected in heparinized containers. Before and after the experiments, as well as every 15 min during the actual measurements, blood samples of the circulating blood were taken for analysis. We determined the hemoglobin content [Hb (g/l)] and the oxygen saturation [HbO$_2$ (%)] by employing a hemoximeter (OSM3, m/s Radiometer, Copenhagen, Denmark) for prompt analysis to ensure constant conditions throughout the experiment. The oxygenation (HbO$_2$) of the circulating blood was maintained at a constant level (at 15–30%, sample dependent) within 1% as a result of the air-tight circulation setup. The saturation level was comparatively low because of the specific oxygen binding properties of hemoglobin in bovine blood.[22] However, to maximize the amount of light transmitted through the blood cuvette in the imaging experiments conducted at 633 nm we saturated the blood with oxygen before the recordings were made. The Hb values varied naturally in the range 110–150 g/l, which corresponds to a Hct of 30−41% based on the average hemoglobin concentration in a single bovine cell (370 g/l; normal range, 350–390 g/l).[17] In addition, the degree of hemolysis was investigated before and after some of the flow experiments, as an indicator of RBC damage. The analysis was made by light-absorption measurements of plasma collected after the blood sample was centrifuged. No significant hemolysis could be detected as a result of circulating and stirring the blood.

B. Imaging the Cell Distribution

Recordings of three blood samples were collected with a 50-ms exposure time. The blood flow rate varied from 0 and 400 ml/min in steps of 50 ml/min, which corresponded to shear rates of 0−1600 s^{-1} at the cuvette wall. The images were all preprocessed by subtraction of the dark-field background. We formed a difference picture from each flow recording by subtracting the corresponding recording of stationary blood. The resultant image was median filtered to remove spike noise and then mean-value filtered to smooth remaining noise. Both filtering kernels were 3 × 3 pixels in size. Pixel values below

Fig. 3. Bovine RBC spheroid equivalents for the T-matrix computations, representing the different morphological conditions studied experimentally. We modeled the effect of cell alignment by varying the orientation of the symmetry axis of the RBC spheroid relative to the incident beam (arrows) from (a) 0° (oblate, $a/b = 0.617$, $x = 16.36$) to (b) 90° (oblate, $a/b = 0.617$, $x = 16.36$). (c) Model of cell-elongation influence (prolate, $a = 2.625$, $a/b = 1.369$, $x = 27.83$).
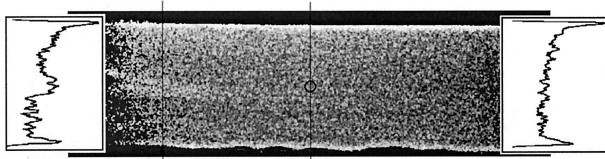
Fig. 4. Processed CCD image of the relative difference in transmittance (633 nm) of flowing (400 ml/min) and nonflowing blood. Bright areas correspond to higher transmittance under flowing conditions compared with nonflowing; dark areas to weaker transmittance; and medium gray to no significant difference. The blood was flowing from left to right. The circle shows the optical probe position, and the traces show the intensity along the two vertical lines indicated.

a threshold were set to zero to give a clear background level. The threshold value was set by visual inspection, so most of the noise was removed from the stationary sides of the cuvette. We finally normalized the result by dividing pixel by pixel with the stationary-blood image.

C. Integrating Sphere Measurements

Transmittance and reflectance spectra were collected for seven whole-blood samples. For each sample the flow was varied from 0 to 400 ml/min in steps of 100 ml/min, corresponding to a wall shear rate in the range $0–1600$ s^{-1}. Spectra were collected at each shear rate with an integration time of 15–30 s. Steady-state spectra were recorded 6 min after the flow was stopped to forestall the influence of any transient postflow phenomena.

The integration time required for acquisition of the T and R spectra was too long to permit the study of aggregation formation after the flow was stopped. We were therefore motivated to investigate the variations in the T and R signals versus time by means of a lock-in detection technique that permitted faster data sampling. The signals following flow stop were recorded for four blood samples.

5. Results

A. Cell Distribution in the Cuvette

No speckle patterns were observed in the transmitted light, indicating that most of the coherence properties were lost because of scattering in the cuvette. Figure 4 shows an image in terms of the difference in transmitted intensities obtained for stationary and flowing blood at 400 ml/min. Thus it presents the difference between two exposures. Bright areas indicate that the transmittance was higher for flowing blood than for stationary; medium gray, that there was no difference between the two conditions; and dark regions, that the transmittance was lower for blood in motion. A weak bright band corresponding to higher transmittance can be discerned in the central part, starting at the inlet of the flow cuvette and fading away toward the center of the cuvette. There is also an increase in transmittance immediately at the edges of the cuvette, clearly shown in the inten-
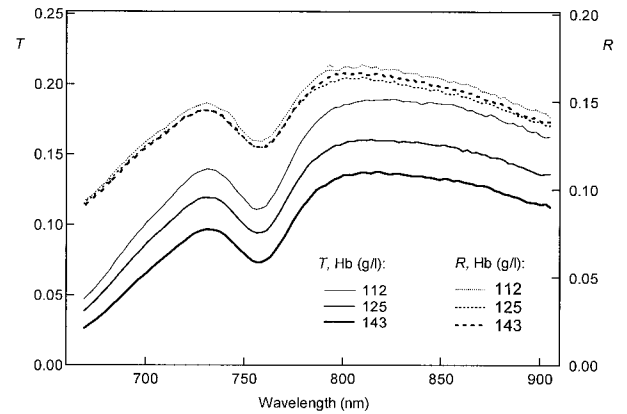
(a)
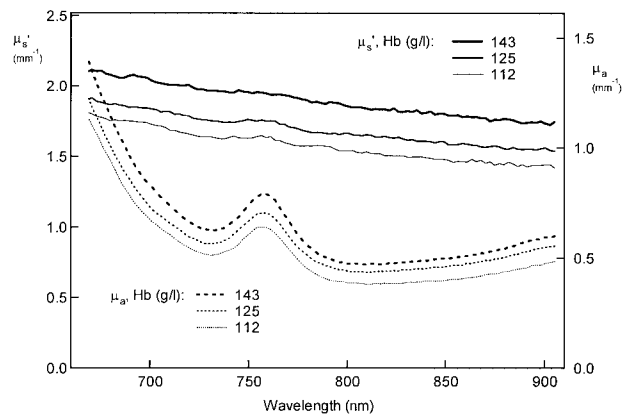
(b)

Fig. 5. (a) Transmittance T and reflectance R spectra for three blood samples with Hb contents of 112, 125 and 143 g/l. The blood was flowing at 200 ml/min, corresponding to a shear rate of 800 s^{-1}. (b) Reduced scattering and absorption coefficients were obtained from the data in (a) by means of an inverse Monte Carlo method.

sity profile to the right of the image, that possibly is due to the shift in shear rate at the cuvette wall and its effect on the cell orientation. The intensity profile in the central region, probed in the integrating sphere measurements, is flat.

B. Influence of Cell Orientation and Elongation: Measurements

Typical spectra of T and R, collected from flowing whole blood, are presented in Fig. 5(a). Spectra for three different blood samples are displayed: Hb = 112 g/l (HbO$_2$ = 25.4%), Hb = 125 g/l (HbO$_2$ = 28.8%), and Hb = 143 g/l (HbO$_2$ = 27.3%), all showing a dip at approximately 760 nm originating from the absorption of light by deoxygenated hemoglobin. The blood was flowing at 200 ml/min in all cases, corresponding to a wall shear rate of 800 s^{-1}. From this figure it is clear that T increases with decreasing Hb over the entire spectral range, whereas the influence on R is less pronounced. The corresponding optical properties μ_s' and μ_a evaluated by the inverse Monte Carlo model are
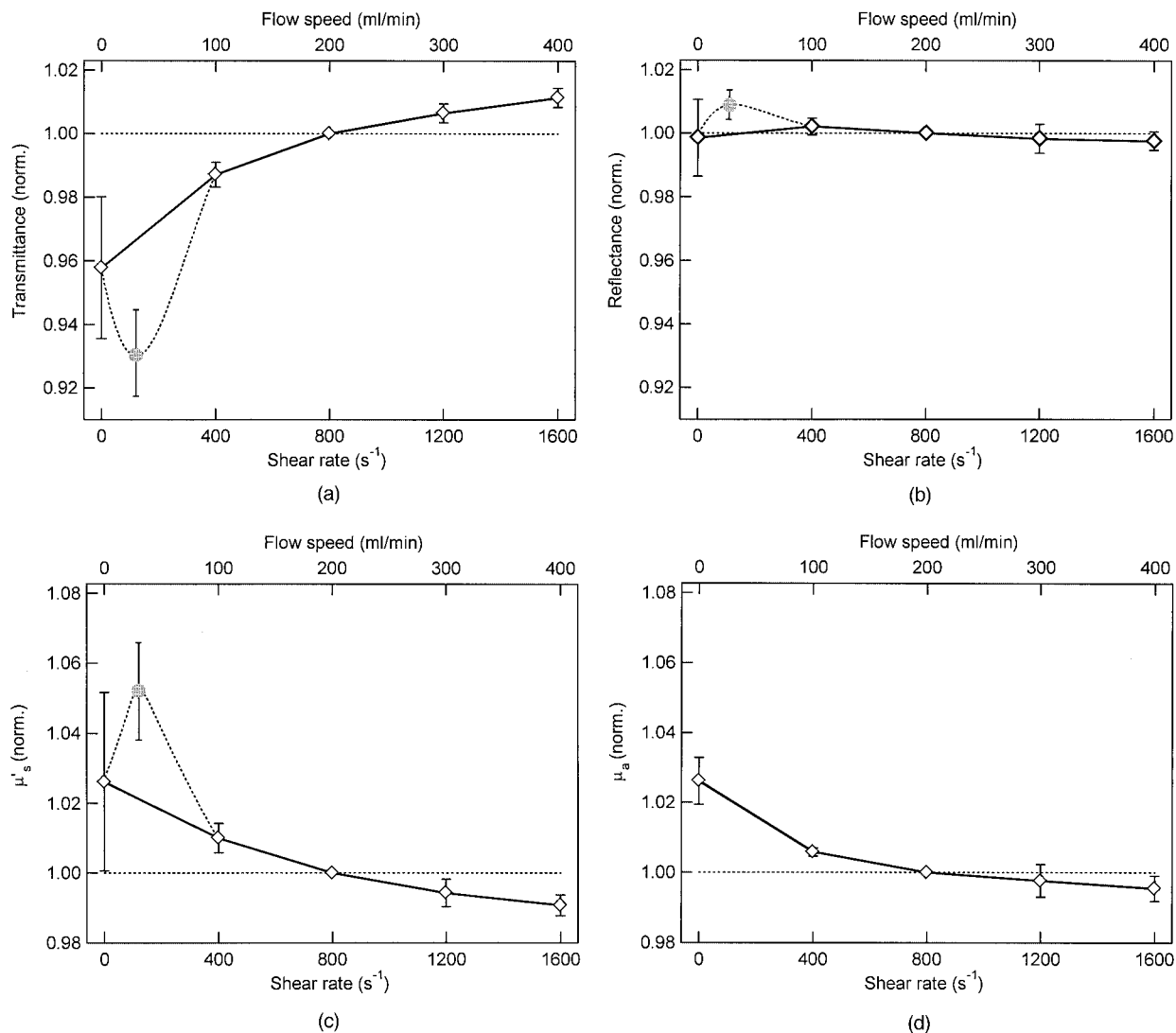
Fig. 6. (a) Transmittance, (b) reflectance, (c) scattering, and (d) absorption at 800 nm versus applied shear rate. The average values and standard deviations of seven samples with values of Hb ranging from 112 to 145 g/l are shown. The optical signals were normalized at a shear rate of $800 \, \text{s}^{-1}$. Data represented by the solid curves were collected with increasing shear rates at the discrete points shown. The dashed curves were interpolated from the results shown in Fig. 7; i.e., data continuously collected after flow stop.

presented in Fig. 5(b). Both the scattering and the absorption properties increase in a consistent manner as Hb (Hct) increases.

The spectra shown in Fig. 5 were recorded not only at 200 ml/min but also at various flow speeds in a range corresponding to maximum shear rates of $0-1600 \, \text{s}^{-1}$. This high-shear-rate regime ensured that the RBCs did not form aggregates but were aligned with the flow and elongated to various degrees. Because variations in the shear rate did not cause any changes in the spectral shape, each spectrum was well represented by its value at 800 nm. Figure 6 clearly illustrates the effect of shear rate on the four properties T, R, μ_s', and μ_a, all normalized at $800 \, \text{s}^{-1}$. The data were compiled from seven samples with values of Hb ranging from 112 to 145 g/l. The error bars show that the measurements varied the most for stationary blood, whereas the data were

consistent when the blood was flowing. There was no correlation between Hb and the magnitude of change in the regimes investigated. All curves show an asymptotic behavior when the shear rate was increased. The transmittance varies the most, with an increase of $6 \pm 2\%$ from 0 to $1600 \, \text{s}^{-1}$. The reflectance exhibits a less pronounced, though significant, decrease of $0.4 \pm 0.2\%$ with increasing shear rate from 400 to $1600 \, \text{s}^{-1}$. The corresponding scattering and absorption coefficients both decrease with increasing shear rate. The absorption and reduced scattering coefficients are compared in Table 1 for shear rates 0, 400, and $1600 \, \text{s}^{-1}$; each rate is representative of a cell's morphological condition: aggregated, aligned, and elongated RBCs, respectively. Alignment of the randomly oriented cells decreases the absorption coefficient by $2.4 \pm 0.1\%$ and the reduced scattering coefficient by $4.0 \pm 0.4\%$. Elonga-

Table 1. Average Values and Standard Deviations of the Relative Change in Experimentally Measured Optical Properties of Whole Blood

	Property	
RBC Morphology	μ_a (%)[a]	μ_s' (%)[a]
Aggregated	1.1 ± 0.2	-4.2 ± 0.8
Randomized	0.0 ± 0.2	0.0 ± 1.4
Aligned	-2.4 ± 0.1	-4.0 ± 0.4
Elongated	-3.4 ± 0.4	-5.8 ± 0.3

[a]Data are given relative to optical properties measured for randomly oriented RBCs.

tion reduces μ_a and μ_s' another 1% and 1.8%, respectively, as listed in Table 1.

C. Influence of Aggregate Formation: Measurements

We investigated the optical response to loss in alignment of the RBCs followed by formation of aggregates by monitoring T and R with a lock-in detection technique versus time after the blood flow was stopped. Average values of time-dependent measurements from four blood samples are presented in Fig. 7. At time zero, the blood was flowing at 200 ml/min, corresponding to a shear rate of 800 s^{-1}. After 20 s on the time scale shown, the pump was turned off and the blood was at rest for 10 min, allowing the RBCs to form aggregates. Finally, the flow was resumed to 200 ml/min, shown for the last 20 s on the time axis in Fig. 7. The signals exhibit strong changes instantaneously after the flow is stopped. Steady-state values are then reached after approximately 6 min. In terms of optical properties, the observed phenomena correspond to instant increases in the absorption and the scattering coefficients in the disorientation phase of 3.0 ± 0.2% and 5.2 ± 1.4%, respectively, compared to values obtained for flowing blood at 800 s^{-1}. Whereas the absorption continues to increase by 1.1 ± 0.2% to a steady-state value, the scattering slowly drops by 4.2 ± 0.8%. Monitoring the signals for as long as an hour yielded no significant change after the plateau was reached. The curves also indicate a slight overshoot when the pumping was resumed after 10 min, indicating a disorientation phase, but the signals quickly settled back to approximately the same levels as those before the flow was stopped.

D. T-Matrix Computations

For comparison with the experimental data, light-scattering computations of oblate- and prolate-shaped cells were made. Both the scattering and the absorption cross sections are significantly influenced by cell orientation and elongation. To permit comparison with experimental data we computed the reduced scattering cross section as $\sigma_s(1 - g)$. The difference in the optical parameters between aligned and randomly oriented cells was evaluated; the latter were obtained from an equivalent power-law distribution [Eq. (5)] of the optical properties of spheres. The results are listed in Table 2. Randomly oriented
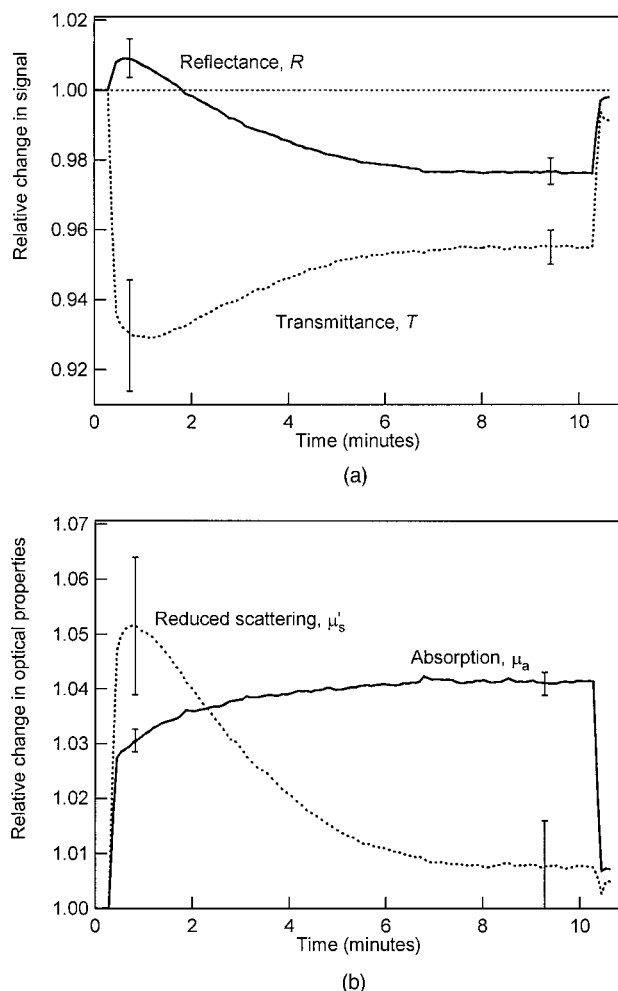

Fig. 7. (a) Light transmittance and reflectance as well as (b) reduced scattering and absorption coefficients measured by means of lock-in detection, with a sample rate of 1 sample/s. During the first 20 s the blood was flowing at 200 ml/min (800 s^{-1}), after which the pump was turned off. The recording on nonflowing blood continued for another 10 min, after which the flow at 200 ml/min was resumed. The signals are normalized with respect to the average value of data collected during the first 20 s. Average values and standard deviations for four blood samples are shown.

rouleau strings of 2–15-cell length were also modeled by the power law distribution approach. Results obtained for the aggregated cells are specified as effective reduced cross sections per cell for the 10-cell rouleau. Whereas the effective absorption cross section per cell is hardly affected by the aggregation, the cellular scattering power is reduced as increasing numbers of cells form the aggregate until a critical aggregate size of approximately five cells is reached, as shown in Fig. 8. Further increase of the aggregate size has a minor influence on either of the effective cross sections. When the orientation of the oblate-shaped cell is varied relative to the incident beam, the scattering has its highest degree of asymmetry ($g = 0.991$–0.992) when the oblate-shaped cell is oriented with its symmetry axis at 0–15 deg relative to the incident

Table 2. Optical Properties Obtained from T-Matrix Computations of Spheroids, Modeling the Listed Morphological Conditions of RBCs[a]

RBC Morphology	Spheroid	Property			
		σ_a (μm^2)	$\sigma_s{}'$ (μm^2)	σ_s (μm^2)	g Factor
Aggregated	Large prolate	0.057 ($-$0.06%)	0.19 ($-$26%)	25 ($-$2.0%)	0.992 (0.25%)
Randomized	Oblate	0.057 (0%)	0.26 (0%)	26 (0%)	0.990 (0%)
Aligned	Oblate	0.054 ($-$4.7%)	0.18 ($-$30%)	21 ($-$18%)	0.991 (0.15%)
Elongated[b]	Prolate	0.056 (2.0%)	0.26 ($-$30%)	25 ($-$0.69%)	0.989 (0.44%)

[a]The cross sections obtained for the 10-cell aggregate, modeled as a large prolate at random orientation (first row), are given per cell. The radius along the symmetry axis of the RBC volume-equivalent prolate (last row) was elongated by 5%. The relative differences, relative to the case of randomly oriented cells, are given in the parentheses for each property. However, the relative changes for the elongated prolate (last row) are instead given relative to the nonelongated prolate.

[b]The relative differences for the elongated prolate are given relative to the nonelongated prolate.

beam (data not shown). The lowest g factor (0.988) is obtained instead at an orientation angle of 90 deg, i.e., when the cell faces its highly curved surface toward the incident beam [Fig. 3(b)]. At this orientation the scattering and absorption cross sections both exhibit their maxima (28.7 and 0.0598 μm^2). When the symmetry axis of the oblate instead coincides with the beam direction, as for aligned RBCs in the flow cuvette being used, the cross sections are minimized (21.1 and 0.0541 μm^2, respectively, as listed in Table 2). The reduced scattering cross section shows an orientation dependence similar to that of the regular cross section. The dependence of the absorption and reduced scattering cross sections on orientation is shown in Fig. 9. We modeled the elongation along one of the two major axes of a RBC by increasing the radius of a prolate along its symmetry axis from 2.5 to 2.65 μm in steps of 0.025 μm while keeping the volume constant. A 5% increase resulted in a higher absorption cross section and g factor, accompanied by a lower scattering cross section (Table 2). The decrease in the reduced scattering cross section with elongation can be attributed mainly to a significant change in the factor $(1 - g)$.

6. Discussion

To be able to vary the cell elongation and orientation in a well-controlled manner, it was essential to ascertain that laminar flow was established at the measurement site in the cuvette. At a tubular expansion similar to that of the cuvette used, the RBCs tend to swirl in vortices close to the cuvette wall immediately following the inlet, as illustrated by Karino and Goldsmith.[23] However, in the central region of the cuvette, corresponding to our measurement site, the mainstream was characterized as homogeneous with no eddies, i.e., as a close to laminar flow. This matches well the band of increased transmittance, stretching from the inlet toward the outlet of the cuvette, that can be observed in the CCD image in Fig. 4. The increased transmittance can hardly originate from a reduced cell concentration but is most likely caused by the higher degree of cell alignment and elongation associated with the central mainstream. This result is consistent with the increase in transmittance observed as a result of the increasing number of aligned and elongated RBCs when the flow rate of blood in motion is increased.[6,24–26] The general consensus deduced
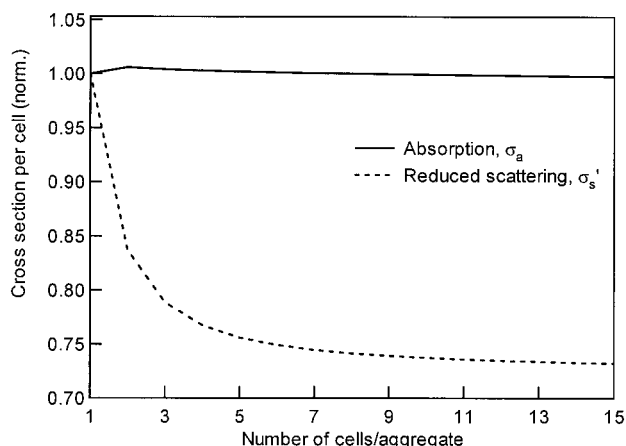

Fig. 8. Reduced scattering and absorption cross sections per cell with increasing aggregate size. The data were obtained from scattering computations of prolate-shaped aggregates, represented by a power-law distribution of spheres.
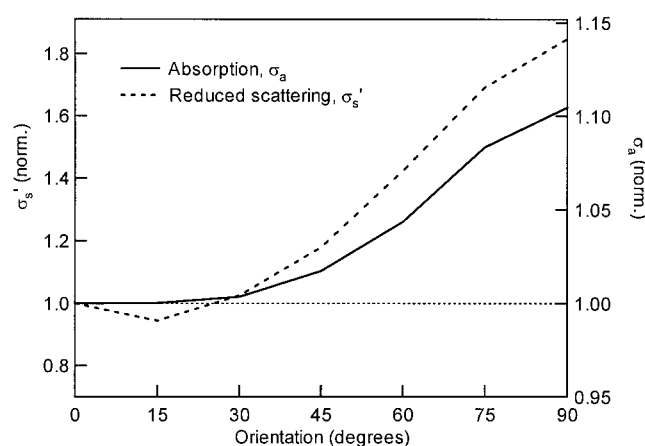

Fig. 9. Reduced scattering and absorption cross sections of the oblate-shaped RBC spheroid [Figs. 3(a) and 3(b)] with increasing angle between the symmetry axis and the incident beam. Note the different scales on the vertical axes.

from these studies is that transmittance and reflectance exhibit a bimodal character with a minimum and a maximum, respectively, at a shear rate of ~ 100 s^{-1}.[26] The minimum of the transmittance in microscopy studies was correlated with the presence of disaggregated and randomly oriented RBCs and increased again during the aggregation phase.[5,6] These results correspond well to those presented in Figs. 6(a) and 6(b). The minimum or maximum of the transmittance or reflectance here was obtained immediately after flow stop with disaligned though still not aggregated RBCs. This phenomenon is also shown in Fig. 7(a), which is in agreement with the results of studies of the aggregation kinetics of blood.[27]

A better understanding of the origin of the observed optical phenomena, found on a cellular level, is gained by expression of the measured optical signals in absorption and scattering coefficients at the various cell morphological conditions. From Figs. 6(c) and 6(d) it is clear that the bimodal properties of the transmittance and reflectance can be entirely attributed to the corresponding character of the scattering properties. The highest value of the reduced scattering coefficient was, as for the reflectance, found immediately following flow stop when the RBCs were randomly oriented. Cell morphology associated with higher degrees of organization, such as aggregated and aligned RBCs, exhibited lower scattering coefficients, as explained by the T-matrix computations. They confirm that aggregation of RBCs reduces the scattering efficiency per cell (Fig. 8). This continues until a critical size of the aggregate has been reached, at approximately five RBCs. The RBC aggregates here were modeled as elongated prolates (radius along the symmetry axis, 2–15 cells), which was justified by the negligible influence of the cell membrane on the scattering properties.[20,21] The T-matrix computations also confirm that spatial orientation of RBCs corresponding to that of aligned cells (symmetry axis along the incident probe beam) provides a lower scattering cross section than other geometries (Fig. 9). Thus, increasing cell alignment will reduce the average scattering efficiency compared with that of an ensemble of randomly oriented cells, as observed experimentally.

In contrast to the reduced scattering cross section, the absorption coefficient increases continuously from high shear rates down to steady state, approximately 6 min after flow stop. The relatively long time required for reaching steady state after flow stop, compared with that for human blood, can probably be attributed to the slow aggregation process that is characteristic of bovine blood.[28] Only a minor change in μ_a (1%) is observed after the pump was switched off [Fig. 7(b)], whereas the major change occurred during the cell-disalignment phase when the shear rate decreased. The increase in absorption coefficient following the flow stop, as well as the fact that it reaches a steady-state value, shows that cell settling in the thin cuvette was negligible. Instead, the minor change in μ_a is in good agreement with the T-matrix computations, showing that the cellular absorption cross section is hardly affected by the cluster formation (Fig. 8). The reason is that particles of this size and relatively low absorption properties exhibit a σ_a value proportional to the particle volume,[29] which remains the same at cell aggregation. The stronger effect on the absorption coefficient observed experimentally during the cell disalignment is also in accordance with the T-matrix computations. The smallest absorption cross section was obtained when the symmetry axis of the RBC equivalent spheroid coincided with the direction of the incident beam (Fig. 9), an orientation that corresponds to that of a perfectly aligned cell. Cells spatially oriented in all other directions contribute positively to the average absorption efficiency. Hence, disalignment increases the absorption coefficient.

In all, the influence of cell morphological properties on absorption and scattering coefficients of whole blood can be predicted and understood qualitatively from T-matrix computations of RBC equivalent spheroids. However, the relative change in the scattering properties observed experimentally is six times less than that predicted by the computations. Neighboring cells do not scatter independently in whole blood and may have a certain contact area, reducing the scattering efficiency per cell (see Fig. 8) that is already under disaggregated conditions. A relatively less pronounced decrease in scattering efficiency during the actual aggregation process therefore seems reasonable. Better theoretical predictions are expected when collective (also referred to as cooperative) scattering effects from neighboring cells are incorporated. Also, the effect of cell alignment is experimentally less significant than in the computations. Because of the high concentration of RBCs we cannot expect the cells to be truly randomly oriented immediately after flow stop or to be perfectly aligned in the so-called aligned condition (400 s^{-1}). Thus the difference in the average scattering coefficients of the two conditions is reduced.

Whereas collective scattering phenomena, and thus the cell-to-cell organization, must be considered for good quantitative agreement between theoretically and experimentally obtained scattering properties of whole blood, the single-particle model seems to handle the effect of cell morphological changes on the absorption properties quantitatively fairly well also. The relative change in absorption cross section (T-matrix computations) of aligned and elongated spheroids is of the same magnitude as that measured. According to the T-matrix computations, the alignment of cells reduces the absorption cross section by 5%, and the elongation increases it by 2%. What we observe experimentally (-3% change) can thus be interpreted as a combination of cells that are merely aligned and cells that are also somewhat elongated.

7. Conclusion

We have shown that cell shape and secondary cell organization have important effects on the optical properties of blood. At low shear rates, when RBCs in whole blood are randomly oriented, the scattering properties measured by the integrating sphere method are significantly higher than both zero and high shear rates, conditions that correspond to a higher degree of organization. In stationary blood, RBCs are organized by aggregation; and in the high-shear-rate regime, as a result of cell alignment and elongation. The absorption properties are also slightly increased. Whereas most of the changes in the absorption properties can be explained by changes in the primary cell morphology, according to the good agreement between the experimentally obtained and T-matrix (single particle scattering) computed results, cell-to-cell organization and its effect on collective scattering effects must be taken into account for good theoretical predictions of the scattering properties of whole blood. From this it follows that optical properties obtained from measurements of diluted blood cannot be extrapolated to those of whole blood.

References

1. H. Schmid-Schönbein and R. Wells, "Fluid drop-like transition of erythrocytes under shear," Science **165**, 288–291 (1969).
2. H. Schmid-Schönbein, K. A. Kline, L. Heinrich, E. Volger, and T. Fischer, "Microrheology and light transmission of blood. III. The velocity of red cell aggregate formation," Pflügers Arch. **354**, 299–317 (1975).
3. H. L. Goldsmith and J. C. Marlow, "Flow behavior of erythrocytes. II. Particle motions in concentrated suspensions of ghost cells," J. Colloid Interface Sci. **71**, 383–407 (1979).
4. J. Goldstone, H. Schmid-Schönbein, and R. Wells, "The rheology of red blood cell aggregates," Microvasc. Res. **2**, 273–286 (1970).
5. H. Schmid-Schönbein, E. Volger, and H. J. Klose, "Microrheology and light transmission of blood. II. The photometric quantification of red cell aggregate formation and dispersion in flow," Pflügers Arch. **333**, 140–155 (1972).
6. H. L. Goldsmith, "The microrheology of red blood cell suspensions," J. Gen. Physiol. **52**, 5s–28s (1968).
7. M. Hammer, D. Schweitzer, B. Michel, E. Thamm, and A. Kolb, "Single scattering by red blood cells," Appl. Opt. **37**, 7410–7418 (1998).
8. A. Roggan, M. Friebel, K. Dörschel, A. Hahn, and G. Müller, "Optical properties of circulating human blood in the wavelength range 400–2500 nm," J. Biomed. Opt. **4**, 36–46 (1999).
9. W. Steenbergen, R. Kolkman, and F. F. M. de Mul, "Light-scattering properties of undiluted human blood subjected to simple shear," J. Opt. Soc. Am. A **16**, 2959–2967 (1999).
10. M. Hammer, A. N. Yaroslavsky, and D. Schweitzer, "A scattering phase function for blood with physiological haematocrit," Phys. Med. Biol. **47**, N65–N69 (2001).
11. L. Wang, S. L. Jacques, and L. Zheng, "MCML—Monte Carlo modeling of light transport in multi-layered tissues," Computer Methods Programs Biomed. **47**, 131–146 (1995).
12. A. N. Yaroslavsky, I. V. Yaroslavsky, T. Goldbach, and H.-J. Schwarzmaier, "Influence of the scattering phase function approximation on the optical properties of blood determined from the integrating sphere measurements," J. Biomed. Opt. **4**, 47–53 (1999).
13. P. W. Barber and S. C. Hill, *Light Scattering by Particles: Computational Methods* (World Scientific, Singapore, 1990).
14. A. M. K. Nilsson, P. Alsholm, A. Karlsson, and S. Andersson-Engels, "T-matrix computations of light scattering by red blood cells," Appl. Opt. **37**, 2735–2748 (1998).
15. H. Schlichting, *Boundary-Layer Theory* (McGraw-Hill, New York, 1968).
16. A. M. K. Nilsson, R. Berg, and S. Andersson-Engels, "Measurements of the optical properties of tissue in conjunction with photodynamic therapy," Appl. Opt. **34**, 4609–4619 (1995).
17. P. Rogers, B. Earley, J. Larkin, and M. Munnelly, "Biochemical variables and trace element analyses—Workshop for Animal Health Professionals, 09-09-1999 (Grange Research Centre, Dunsany, Co. Meath, Ireland, 2002), http://www.research.teagasc.ie/grange/lab_vars.htm.
18. D. H. Tycko, M. H. Metz, E. A. Epstein, and A. Grinbaum, "Flow-cytometric light scattering measurement of red blood cell volume and hemoglobin concentration," Appl. Opt. **24**, 1355–1364 (1985).
19. N. V. Shepelevich, I. V. Prostakova, and V. N. Lopatin, "Light-scattering by optically soft randomly oriented spheroids," J. Quant. Spectrosc. Radiat. Transfer **70**, 375–381 (2001).
20. R. A. Meyer, "Light scattering from red blood cell ghosts: sensitivity of angular dependent structure to membrane thickness and refractive index," Appl. Opt. **16**, 2036–2038 (1977).
21. S. V. Tsinopoulos, E. J. Sellountos, and D. Polyzos, "Light scattering by aggregated red blood cells," Appl. Opt. **41**, 1408–1417 (2002).
22. M. F. Perutz and K. Imai, "Regulation of oxygen affinity of mammalian haemoglobins," J. Mol. Biol. **136**, 183–191 (1980).
23. T. Karino and H. L. Goldsmith, "Flow behaviour of blood cells and rigid spheres in an annular vortex," Philos. Trans. R. Soc. London Ser. B **279**, 413–445 (1977).
24. H. J. Klose, E. Volger, H. Brechtelsbauer, L. Heinich, and H. Schmid-Schönbein, "Microrheology and light transmission of blood. I. The photometric effects of red cell aggregation and red cell orientation," Pflügers Arch. **333**, 126–139 (1972).
25. K. Sakamoto and H. Kanai, "Electrical characteristics of flowing blood," IEEE Trans. Biomed. Eng. **BME-26**, 686–695 (1979).
26. L.-G. Lindberg and P. Å. Öberg, "Optical properties of blood in motion," Opt. Eng. **32**, 253–257 (1993).
27. M. R. Hardeman, J. G. G. Dobbe, and C. Ince, "The laser-assisted optical rotational cell analyzer (LORCA) as red blood cell aggregometer," Clin. Hemorheol. Microcirc. **25**, 1–11 (2001).
28. H. Bäumler, B. Neu, R. Mitlöhner, R. Georgieva, H. J. Meiselman, and H. Kiesewetter, "Electrophoretic and aggregation behavior of bovine, horse and human red blood cells in plasma and in polymer solutions," Biorheology **38**, 39–51 (2001).
29. H. C. van de Hulst, *Light Scattering by Small Particles* (Wiley, New York, 1957).